Journal of Applied Science and Engineering Methodologies
Volume.2, No.3, (2016): Page.346-352
www.scientistlink.com/jasem

# Influence of Calcination on the $TiO_2$ Polymorphs and its Electronic Structure Analysis through Optical Absorption Studies

**S. Sharmila Juliet[1], S. Ramalingom[2], A. Moses Ezhil Raj[1]***
[1]Department of Physics &Research Centre, Scott Christian College (Autonomous), Nagercoil, India.
[2]Department of Physics, Vivekananda College, Agasteeswaram-629701, India.

**Abstract:** Pure nanocrystalline titanium Oxide ($TiO_2$) powder has been synthesized by the sol-gel technique using titanium tetra-isopropoxide as the starting precursor. As-prepared samples were calcined at different temperatures, 400, 600, 800 and 900°C. X-ray diffraction (XRD) analysis was used to find the crystalline structure and changes in the polymorphs with calcination. The as-synthesized $TiO_2$ powder dried at 100ºC in air was amorphous. The powder samples calcined at 400 ºC (a=3.788 Å, c=9.499 Å) and 600ºC (a=3.787 Å, c=9.518 Å) revealed only the anatase phase with the tetragonal structure belongs to the space group of $I4_1/amd$-$D_{4h}^{19}$, whereas the sample calcined at 800ºC (a=4.597 Å, c=2.962 Å) exhibited mixed anatase and rutile phases with tetragonal structure. Calcined $TiO_2$ powders at 900 ºC rendered rutile phase with the tetragonal structure and space group of $P4_2/mnm$-$D_{4h}^{14}$ (a=4.599 Å, c=2.963 Å). The Fourier transform infrared spectrometer (FT-IR) was used to confirm the metal-oxide phase formation and to test the presence of any organic residues. The electronic structure of $TiO_2$ has been investigated using the optical absorption spectra based on combined density functional theory and many-body perturbation theory. Absorption edge observed nearer to 410 nm showed the bandgap values between 2.97 and 3·24 eV. Electrical conductivity study was performed to understand the conduction mechanism of the samples and it effect variation with calcination.

---

***Corresponding author**
e-mail: ezhilmoses@yahoo.co.in (A. Moses Ezhil Raj)
Phone: +91 4652 232888 | Fax: +91 4652 229800

## 1. Introduction

Titanium dioxide, also known as Titania, is one among the smart materials due to its proven ability to function as a photocatalyst and facilitate important environmentally beneficial reactions, such as water splitting to generate hydrogen and treating polluted air and water. The nano crystalline titanium dioxide occurs as two important polymorphs, the metastable anatase (tetragonal (4/mmm), $I4_1/amd–D_{19}^{4h}$) and stable rutile crystal system: tetragonal (4/mmm), space group: $P4_2/mnm–D_{14}^{4h}$) [1]. These polymorphs exhibit different properties and consequently different photocatalytic performances. Anatase transforms irreversibly to rutile at elevated temperatures.

Each of the two $TiO_2$ phases is tetragonal, and Mo and Ching and Fahmi *et al.*[2, 3] reviewed their structural properties including crystal structures, space groups, and differences in bond lengths and angles. These two crystal structures can be considered as arrangements of slightly distorted oxygen octahedral elements with a titanium atom at the center of each so that each titanium has an oxygen coordination of six and each oxygen has a titanium coordination of three. The relationship between the two structures has been described in terms of varied orientation among the octahedral chains. The two polymorphs can be generated with six-atom unit cells corresponding to two $TiO_2$ units. Each unit possesses two inequivalent bonds of “apical” and “equatorial” character, such that each titanium atom sees two apical and four equatorial bonds, while each oxygen atom sees one apical and two equatorial bonds. Structural similarities in rutile and anatase lead to similarities in their electronic structure.

The absorption spectrum of a semiconductor defines its possible uses. The useful semiconductors for photocatalysis have a bandgap comparable to the energy of the photons of visible or ultraviolet light, having a value of Eg < 3.5 eV. There have been reported values in the literature from 2.86 to 3.34 eV for the anatase phase, the differences being attributed to variations in the stoichiometry that depend on synthesis, the impurities content, the crystalline size and the type of electronic transition [4, 5]. As a semiconductor material with long-term stability, non-toxic environmental acceptability and broadly low cost availability $TiO_2$ has also been taken into account for photovoltaic applications.

Published by SLGP. Selection and/or peer-review under responsibility of ICISEM 2016. 

However, due to optical gaps slightly above 3 eV (rutile:~ 3.0 eV [6, 7] and anatase: ~3.4 eV [8]), natural $TiO_2$ is only photoactive in the UV region of the electromagnetic spectrum and an inefficient active solar cell material. Still, the material advantages of $TiO_2$ can be used indirectly in technically and economically viable dye-sensitized solar cells [9-11] where it acts as an electron-transporting substrate for a chemisorbed photoactive dye.

Several density functional theory (DFT)-based studies on various $TiO_2$ phases (mainly rutile and anatase) have been published so far [12-19]. The improved description of the electronic structure by hybrid-functional schemes has been discussed in the literature [20-24]. Recently, some studies have investigated many-body effects (self-energy corrections and excitonic effects) on the optical absorption [25] of rutile and anatase. Lawler et al. investigated the birefringence of the oxides $TiO_2$ including excitonic effects from the solution of the Bethe–Salpeter equation (BSE). Chiodo et al. as well as Kang and Hybertson [26, 27] both applied many-body perturbation theory (MBPT) methods (i.e. GW approximation and BSE) to calculate optical properties. Their results have clearly demonstrated the necessity of quasiparticle corrections to reproduce experimental photoemission bandgap data as well as the importance of including electron–hole interaction in the simulation of the optical response of the two tetragonal polytypes rutile and anatase. In this work optical parameters are evaluated in context of the bandgap of the synthesized $TiO_2$ samples by the sol-gel method using titanium tetra isopropoxide as a starting precursor.

## 2. Experimental

$TiO_2$ nano powders has been prepared using Titanium tetraisopropoxide $[Ti\{OCH(CH_3)_2\}_4]$ as the starting precursor. In a typical preparation, 8 ml. of precursor was dissolved in 50 ml ethanol under constant magnetic stirring. The sol obtained after 45 min. was converted into gel by adding 100 ml of de-ionized water. Obtained white precipitate was filtered and washed with distilled water for three times to remove impurities. Finally, the powders were dried in air at 100ºC for 1h, and then calcined at 400, 600, 800 and 900ºC for 2h in a muffle furnace and named $TiO_2$, $TiO_2$ 400, $TiO_2$ 600, $TiO_2$ 800 and $TiO_2$ 900 respectively for the resultant powder samples. Structural investigations were performed using X-ray diffraction recorded in the PANalytical 3040 X'pert-Pro diffractometer. FTIR spectrum was recorded in the spectral range of 400-4000 $cm^{-1}$ with a Nexus 670 spectrometer. The optical absorption spectra were recorded in the wavelength range 200-2500 nm using Varian Cary 5000 spectrophotometer. For electrical measurements the powders were uniaxially pressed into pellets of 13 mm in diameter, 2 mm in thickness using Hydraulic pellet press of type KP with the load of 5 tones and sintered at 200°C for 1h with a heating rate of 10°C per min and the DC conductivity was measured by the electrical resistance measurement system from room temperature to 150°C using high precisions electrometers.

## 3. Results and Discussion

From the XRD technique, the as prepared $TiO_2$ nano powder dried in air showed amorphous structure with a broad and low intensity pattern. Fig. 1 shows the XRD patterns of the $TiO_2$ calcined samples at 400 and 600°C along with JCPDS standard for comparison.

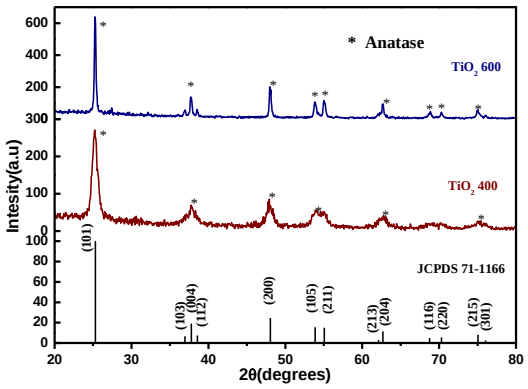


**Fig. 1 XRD patterns of anatase $TiO_2$ nanopowders calcined at 400ºC and 600ºC**

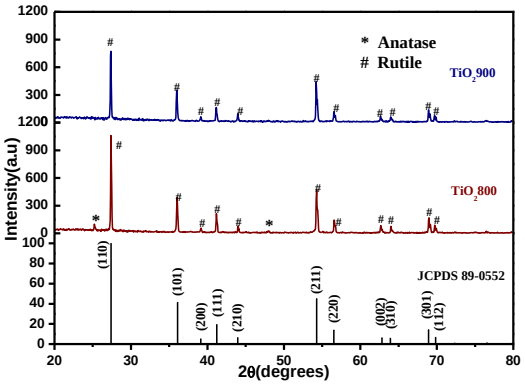


**Fig. 2 XRD patterns of rutile $TiO_2$ nanopowders calcined at 800ºC and 900ºC.**

All the observed peaks can be indexed for the tetragonal anatase phase (JCPDS file no.: 71- 1166). The maximum intensity diffraction peaks at 2θ = 25.25º and 48º strongly confirm the formation of $TiO_2$ in the anatase phase without the influence of other phases like rutile and brookite. The titanate phase could transform to anatase phase at the calcination temperature higher than 400°C. Broad diffraction lines of $TiO_2$ nano powder calcined at 400°C entail small crystallite size. As the calcination temperature increases from 400 to 600°C the peak intensities increased indicating the improvement of crystallization of anatase phase and the peak width decreases that show the increase in the crystallite size. With further increase in the calcination temperature from 600 to 800°C, the transition from anatase to rutile starts. Fig. 2 clearly shows the phase transition from anatase to rutile. $TiO_2$ 800 has both phases with corresponding rutile peaks at 2θ =27.34º and 54.2º along with peaks at 2θ =25.25º and 47.97º that are assigned to the anatase phase. As the calcination temperature increases from 800 to 900°C, the anatase phase totally vanishes and has transformed completely to the rutile phase with the increase in intensity. Finally the $TiO_2$ powder sample calcined at 900°C has rutile phase alone. The indexed peak and from its angular position, the lattice parameters can be evaluated. The crystallite sizes of calcined powders were obtained using the Scherrer's formula [28]. Scherrer plot also be constructed to verify the crystallite size. The microstrain values are obtained from the constructed Williamson-Hall plot [29, 30]. Obtained microstructural data are listed in Table 1.

**Table 1: Structural parameters $TiO_2$ nanopowder samples**

| Sample Details | Crystallite Size, D (nm) | | | Lattice parameters (Å) | | Microstrain (ε) x$10^{-4}$ | Density ρ (g/$cm^3$) |
|---|---|---|---|---|---|---|---|
| | Scherrer's Formula | Scherrer's Plot | Williamson -Hall plot | a | c | | |
| $TiO_2$400 | 14.66 | 16.86 | 9.81 | 3.788 | 9.499 | -15.9 | 3.89 |
| $TiO_2$600 | 41.00 | 42.22 | 33.21 | 3.787 | 9.518 | -4.32 | 3.89 |
| $TiO_2$800 | 81.74 | 85.69 | 44.02 | 4.597 | 2.962 | -8.78 | 4.24 |
| $TiO_2$900 | 74.76 | 81.82 | 86.20 | 4.599 | 2.963 | -0.20 | 4.23 |

Calculated crystallite size using Williamson-Hall plot is the precise value of the crystallite size because peak width is considered for both size effect and lattice strain. Moreover, it is observed that the crystallite size increases with calcination temperature due to agglomerisation. As the calcination temperature is increased, the grain size and proportion of the rutile phase also increased, indicating that the higher calcination temperature favoured the formation of larger crystallites and the rutile phase of $TiO_2$. The slight variation in the lattice parameter on increasing calcination temperature indicates the presence of compressive stain in the lattice. The microstrain decreases as the crystallite size increases. The density data also clearly indicates the phase change.

Fig. 3 shows the FTIR spectra of as-prepared and calcined $TiO_2$ nanocrystals. As-prepared samples exhibits a broad band in the measured range 3370-3097$cm^{-1}$ which can be assigned to the stretching vibration of the hydroxyl (O–H) group [31]. The low intensity of these peaks in the calcined samples indicates the removal of large portion of adsorbed water from $TiO_2$. The characteristic absorption peak of (OR) group of titanium isopropoxide, which is the precursor of the sols, is in range 1085–1050 $cm^{-1}$[32]. Owing to the fact that absence of these peaks on annealing confirms that all the four (OR) groups of titanium isopropoxide are removed from the resultant product. Thus, a full conversion in TTIP is obtained by the hydrolysis reaction, resulting in formation of $TiO_2$ particles. The additional peaks in the wavenumber range 1650–1600 $cm^{-1}$ also indicates the incorporation of water in the as-prepared samples. However, these absorption bands are disappeared on heating to 600°C. This indicates that 600°C is the suitable temperature for the formation of anatase phase $TiO_2$ in its purest form.

The appearance of a large broad band in the range 500–900 $cm^{-1}$ with maximum absorption at 515 $cm^{-1}$ is the characteristics of Ti–O–Ti anatase structure [33-36]. The sample $TiO_2$ 800 indicates two additional bands at 521 and 422 $cm^{-1}$ assignable to the stretching of Ti–O–Ti bonds in anatase and rutile respectively [36]. This additional peak indicates the phase transition from anatase to rutile. The disappearence of two additional bands at 521 and 422 $cm^{-1}$ in the $TiO_2$ sample calcined at 900ºC indicates the complete phase transition from anatase to rutile phase.

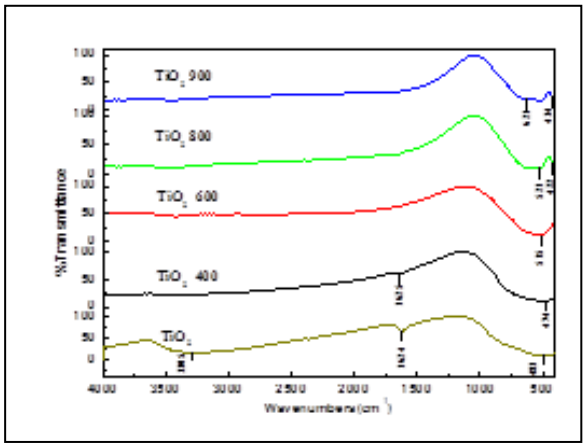


**Fig. 3 FTIR spectra of $TiO_2$ samples**

The absorption spectrum of $TiO_2$ samples are shown in Fig. 4. It can be seen that all samples are strong absorbers in the ultraviolet region. The absorption edge of annealed $TiO_2$ samples moved to longer wavelength on increasing the calcination temperature. The optical band gap can be estimated from a plot of $(\alpha h\nu)^2$ vs. photon energy ($h\nu$) (Inset of Fig. 4). The intercept of the tangent to the plot will give a good approximation of the bandgap energy for the direct band gap material [40]. The band gap of the $TiO_2$ powder samples varies from 2.97 to 3.24 eV (Table 2). Obtained band gaps of the rutile and anatase phase are comparable to the reported values of Kang and Hybertson as well as Chiodo et al. [26, 27].

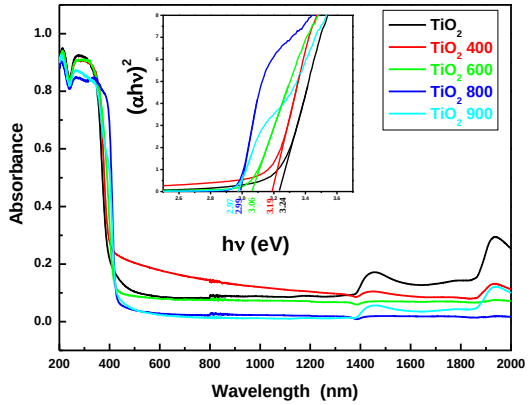


**Fig. 4 Absorbance spectra of $TiO_2$ samples. Inset-Tauc plot**

| Sample Details | Optical Bandgap (eV) | Conductivity (mho/m) | Activation Energy (eV) |
|---|---|---|---|
| $TiO_2$100 | 3.24 | $1.32x10^{-9}$ | 0.774 |
| $TiO_2$400 | 3.19 | $2.58x10^{-9}$ | 0.638 |
| $TiO_2$600 | 3.06 | $7.16x10^{-9}$ | 0.623 |
| $TiO_2$800 | 2.99 | $3.24x10^{-10}$ | 0.602 |
| $TiO_2$900 | 2.98 | $4.37x10^{-11}$ | 0.443 |

**Table 2 Optical and electrical data of $TiO_2$ samples**

The optical absorption technique can also be used to determine the type of the $TiO_2$ materials [41]. Optical absorption measurements around 3 eV to 4 eV is an electronic fingerprint for the determination of the materials whether they are crystalline or amorphous. For amorphous materials, the values of the bandgap are above 3.4eV independent of the transition type, which is in agreement with the XRD results. As the prepared materials are crystalline, obtained band gap values are well below 3.4 eV. The variations in band gap values can be attributed primarily to the phase change from anatase to rutile. Even in its anatase phase, the variation in band gap may be the due to the change in the crystalline size of the catalysts [4], as evidenced from the XRD results in the present study.

**Table 3 Theoretical and experimental structural parameters and their band gap energy for $TiO_2$ samples**

| Phase | Method | Lattice Constants | | | *Optical Bandgap Eg (eV)* |
|---|---|---|---|---|---|
| | | a (Å) | b(Å) | c(Å) | |
| **Anatase** | PBE | 3.801 | 3.801 | 9.711 | 2.143 |
| | HSE06 | 3.770 | 3.770 | 9.626 | 3.341 |
| | DFT | 3.782 | 3.782 | 9.502 | 3.2-3.4 |
| | UV | 3.788 | 3.788 | 9.499 | 3.19-3.06 |
| **Rutile** | PBE | 4.641 | 4.641 | 2.970 | 1.802 |
| | HSE06 | 4.593 | 4.593 | 2.953 | 3.083 |
| | DFT | 4.593 | 4.593 | 2.959 | 3.0 |
| | UV | 4.599 | 4.599 | 2.963 | 2.99-2.98 |

To validate the calculation of the optical parameters, it was compared with the hybrid density functional theory (DFT) calculations engaged to calculate the structural and electronic properties of rutile and anatase $TiO_2$ crystals. The theoretical lattice constants and band gap energies are listed in Table 3, along with the experimental data. It can be found that the reported theoretical lattice constants calculated both using the PBE and HSE06 functionals are very close to the experimental values [42, 43]. Obtained theoretical band gap energy values using PPE, HSE06 and DFT functional for the anatase and rutile $TiO_2$ matched well with our optical experimental results. The significant improvement through the hybrid DFT calculations confirms the advantage of this method.

In order to study the mechanisms of conductivity, it is convenient to plot logarithm of the conductivity (σ) as a function of 1000/T. Fig. 5 shows the relation between ln σ and 1000/T for the $TiO_2$ samples. Conductivity measurements were carried out in the temperature range from 30 to 150$^oC$. The plots are further analyzed to calculate the activation energies $E_a$ from the slopes of the straight lines in all the synthesized samples using Arrhenius equation [44]. It is clear from the Fig.5 that the plots are linear for all the samples indicating that the conduction in these samples are due to an activated process having single activation energy in the given temperature range. Further it confirms that the conductivity increases with increase of temperature, such as the general characteristics of the semiconductor. With increasing temperature lead to an increase in the number of electron-hole pairs result in an increased conductivity. The analysis of the conductivity data yields the activation energies of the donor levels, which are given by an Arrhenius plot.

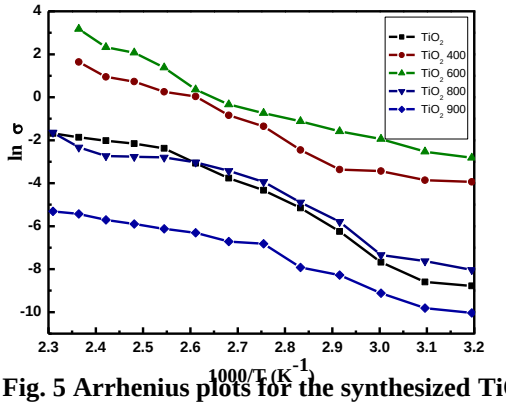


**Fig. 5 Arrhenius plots for the synthesized $TiO_2$ samples calcined at different temperatures**

The conduction mechanism of the activation energy ($E_a$) at the given lower temperatures range is due to carrier excitation into localized state at the edge of the band [45]. All the samples show a perfect

semiconducting behaviour and hence increase in conductivity with increasing temperature as expected. An increase in conductance of as synthesized $TiO_2$ may be ascribed to the presence of adsorbed water molecules on the surface of pure titanium oxide before calcination. The electrical and physical properties of semiconductor metal oxides are mostly affected by the depth of the space charge region within the crystallite or grain. If the size of the particle is smaller, the electrical properties of the material are strongly affected by the surface phenomena. Tang et.al [46] reported that the nano crystalline $TiO_2$ metal oxides with the crystallite size of 20 nm represent such phenomena, where the depletion can develop very well through the entire grain and affect its conductivity. Such homogeneous charge concentration in the crystallite or grain leads to the case of flat band potential. Development of the space charge region in nanocrystalline materials is strongly related to the thermal conditions, thus along with the temperature increase the concentration of electron increases and as a result the width of the depletion layer decreases. In case of large grains, an additional transport from one crystallite or grain to another has to be as well considered [47].

The calculated activation energy of the synthesized $TiO_2$ samples are tabulated as 0.774, 0.638, 0.623, 0.602, 0.443 eV, which decreases with increase in calcination temperature (Table 2). Increase in grain size and thus the decrease in strain values together alters the activation energy. The rutile sample $TiO_2$ 900 has the lowest activation energy of 0.443 eV. Thus the conductivity of prepared samples increases with the temperature significantly due to semiconducting behaviour and also it increases due to the grain size effect while activation energy increases with decrease of grain size.

## 4. Conclusions

Nanoparticulate titanium dioxide was successfully synthesized and its transition to various polymorphs was evidenced from the XRD studies. Interplay of calcination temperature for the transition was understood from the structural parameters. The metal-oxide phase formation and its transition from anatase to rutile was clearly evidenced from the changes in the vibrational bands of the FTIR spectrum. Obtained optical band gap values were compared with the theoretical values obtained through DFT, PBE and HSE06 functionals. Optical DC Conductivity measurement revealed the semiconducting nature of the samples and the variations in the activation energy values were explained based on crystallite size effect.

## References

[1] M Landmann, E Rauls and W G Schmidt, J. Phys. Condens. Matter, 24 (2012) 195503.
[2] S D Mo and W Y Ching, Phys. Rev. B 51 (1995) 13023.
[3] A. Fahmi, C Minot, B Silvi, and M Caus'a, Phys. Rev. B 47 (1993) 11717.
[4] M Hidalgo, M Aguilar, M Maicu, J Navio, G Colon. Catal Today 129 (2007) 50.
[5] F Hossain, L Sheppard, J Nowotny, G Murch, J. Phys. Chem Solids 69 (2008) 1820.
[6] J Pascual, J Camassel and H Mathieu, Phys. Rev. B 18(1978) 6842.
[7] A Amtout and R Leonelli, Phys. Rev. B 51(1995) 6842.
[8] H Tang, F Levy, H Berger and P E Schmid, Phys. Rev. B 52(1995) 7771.
[9] U Bach, D Lupo, P Comte, J E Moser, F Weissortel, J Salbeck, H Spreitzer and M Gratzel, Nature 395 (1998) 583.
[10] M Gratzel, Mater. Res. Soc. Bull. 30(2005) 23.
[11] A Hagfeldt, G Boschloo, L Sun, L Kloo and H Pettersson, Chem. Rev. 110 (2010) 6595.
[12] K M Glassford and J R Chelikowsky, Phys. Rev. B 46 (1992) 1284.
[13] P J Hardman, G N Raikar, C A Muryn, G Vander Laan, P L Wincott, G Thornton, D W Bullett and Dale Padma, Phys. Rev. B 49 (1994)7170 .
[14] M. Mikami, S Nakamura, O Kitao, H Arakawa and X Gonze, Japan. J. Appl. Phys. 39 (2000) L847.
[15] R Asahi, Y Taga, W Mannstadt and A J Freeman, Phys. Rev. B 61 (2000) 7459.
[16] M Calatayud, P Moris anchez, A Beltran, A M Pendas, E Francisco, J Andres and J M Recio, Phys. Rev. B 64 (2001) 184113.
[17] J Muscat, V Swamy and N M Harrison, Phys. Rev. B 65 (2002)224112.
[18] X Wu, E Holbig and G Steinle Neumann, J. Phys. Condens. Matter 22 (2010) 295501.
[19] E Shojaee and M R Mohammadizadeh, J. Phys. Condens. Matter 22 (2010) 015401.
[20] Y Zhang, W Lin, Y Li, K Ding and J Li, J. Phys. Chem.B 109 (2005) 19270.
[21] A Beltran, L Gracia and J Andres, J. Phys. Chem. B 110 (2006) 23417.
[22] B Lee, C Lee, C S Hwang and S Han, Curr. Appl. Phys. 11 (2010) S293.
[23] A Janotti, J B Varley, P Rinke, N Umezawa, G Kresse and C G Van de Walle, Phys. Rev. B 81 (2010) 085212.
[24] P Deak, B Aradi and T Frauenheim, J. Phys. Chem. C 115 (2011) 344.
[25] H M Lawler, J J Rehr, F Vila, S D Dalosto, E L Shirley and Z H Levine, Phys. Rev. B 78 (2008) 205108.

[26] L Chiodo, J M Garcia-Lastra, A Iacomino, S Ossicini, J Zhao, H Petek and A Rubio, Phys. Rev. B 82 (2010) 045207.
[27] W Kang and M S Hybertsen, Phys. Rev. B 82 (2010) 085203.
[28] J I Langford, A J C Wilson, J. Appl. Cryst. 11 (1978) 102.
[29] G K Williamson, W H Hall, Acta Metall. 1 (1953) 22.
[30] P Scardi, M Leoni, R Delhez, J. Appl. Crystallogr, 37 (2004) 381.
[31] G Socrates, John Wiley & Sons, England, (1994) 6, 62 and 237.
[32] G Socrates, Infrared and Raman Characteristic Group Frequencies: Tables and Charts, third ed, John Wiley & Sons Ltd, England. (2001).
[33] G Carja, G Delahay, Appl. Catal. B 47 (2004) 59.
[34] J Yang, H Bai, X Tan, Lian, J. Appl Surf. Sci. 253 (2006) 1988.
[35] C Wen, H Ssu, T Jeou, C Hsin, H Tzu, J. Chemosphere, 66 (2007) 2142.
[36] I R Beattie, T R Gilson, J. Chem. Soc. A (1969) 2322.
[37] J Essick, R Mather, Am J Phys. 61 (1993) 646.
[38] R Willardson, A Beer, Optical Properties of III-V Compounds. Academic Press New York. (1967) 318.
[39] M Dressel, G Gruner, Electrodynamics of Solids Optical Properties of Electron in Matter. Cambridge University Press. (2002) 159.
[40] Y Wang and N Herron, J. Phys. Chem. 95 (1991) 525.
[41] A Welte, C Waldauf, C Brabec, P Wellmann. Thin Solid Films, 516 (2008) 7256.
[42] H Tang, H Berger, P E Schmid and F Levy, Solid State Commun, 92 (1994) 267.
[43] Y Wang, T Sun, D J Yang, H W Liu, H M Zhang, X D Yao and H J Zhao, Phys. Chem. Chem. Phys, 14 (2012) 2333.
[44] M P Rajeeva, C S Naveen, Ashok R. Lamani, V Prasad Bothla, and H S Jayanna, Conf. Proc, 1665 (2015) 050091.
[45] J I Langford and A J C Wilson, J. Appl. Cryst. 11 (1978) 102.
[46] H Tang, K Prasad, R Sanjines, P E Schmid. F Levy, J. Appl. Phys, 75 (1994) 2042.
[47] N Barsan, U Weimar, J. Electroceramics, 7 (2001) 143.